19

Molecular Design of a Chiral Oligomer for Stabilizing a Ferrielectric Phase

Atsushi Yoshizawa and Anna Noji
Department of Frontier Materials Chemistry, Hirosaki University
Japan

1. Introduction

Appearance of ferroelectricity and antiferroelectricity in chiral tilted smectic phases is an interesting phenomenon. It is not only attractive for use in applications to fast-response displays (Goodby et al., 1991; Walba, 1995); it also attracts fundamental interest related to synclinic or anticlinic ordering of the molecules (Lagerwall & Giesselmann, 2006; Lemieux, 2007; Nishiyama, 2010). The frustration between synclinic-ferroelectricity and anticlinic-antiferroelectricity in chiral smectic C phases causes temperature-induced successive phase transitions (Fukuda et al., 1994; Inui et al. 1996; Isozaki et al., 1993; Matsumoto et al., 1999; Osipov & Fukuda, 2000; Sandhya et al., 2009; Takezoe et al., 2010). When ferroelectric and antiferroelectric phases have equal free energy, intermediate ferrielectric sub-phases with a degenerated energy level can appear between ferroelectric and antiferroelectric phases.

At the outset of disclosing antiferroelectric SmC*$_A$ phase in MHPOBC, three other SmC*-like phases were observed (Chandani et al., 1989a). These phases were designated as SmC*$_\alpha$, SmC*$_\beta$, and SmC*$_\gamma$ in order of decreasing temperature (Chandani et al., 1989b), the SmC*$_\beta$ phase was regarded as the oridinary ferreoelectric SmC* phase. Gorecka et al. soon proved that SmC*$_\gamma$ is a ferrielectric phase (Gorecka et al., 1990). Isozaki et al. confirmed that an antiferroelectric subphase might emerge between SmC*$_\beta$, and SmC*$_\gamma$ phases (Isozaki et al., 1992, 1993). Mach et al. reported the first direct structural observation of distinct multilayer periodicities of the subphases using resonant X-ray scattering (March et al., 1998, 1999). They confirmed three-layer and four-layer periodicities, respectively, in what they called Ferri 1 and Ferri 2 phases. Nguyen et al. identified the Ferri 1 as SmCγ* (Nguyen et al., 1994). The Ferri 2 phase was found to have antiferroelectric characteristics (Aoki et al., 1999). Later, the SmC*$_\beta$ of MHPOBC was identified as Ferri 2 phase (Gorecka et al., 2002). At least two ferrielectric phases consisting of three-layer and four-layer unit cells exist. Other ferrielectric subphases induced by successive phase transition have been observed. Fukuda et al. proposed that the subphases are represented as SmC*$_A$(qT), where qT = F/(A+F) (Isozaki et al., 1993). In those equations, F denotes the number of synclinic layers in one periodicity: A represents the number of anticlinic layers in one periodicity. Figure 1 presents illustrations of antiferroelectric phase SmC*$_A$ (0), ferrielectric subphase SmC*$_A$ (1/3), antiferroelectric-like ferrielectric subphase SmC*$_A$ (1/2), and ferroelectric phase SmC*$_A$ (1).

Some theoretical and experimental studies have been undertaken to explain the appearance of ferrielectric phases (Cepic & Zeks, 2001; Cepic et al., 2002; Fukuda et al., 1994; Johnson et al., 2000; Matsumoto et al., 1999; Osipov & Fukuda, 2000; Yamashita & Miyajima, 1993).

Chirality is probably prerequisite for the appearance of the ferrielectric phases. Emelyanenko and Osipov proposed that effective coupling that is determined using a combination of spontaneous polarization, discrete flexoelectric effect, and an initial direct polarization coupling between adjacent layers stabilizes the ferrielectric phases (Emelyanenko & Osipov, 2003). The Emelyanenko-Osipov model predicts only mesophases with periodicity of 8, 5, 7, and 9 layers between SmC* and SmC*$_A$ phases. However, SmC* phase with six-layer periodicity has been discovered (Wang, et al, 2010). The physical origin of long-range interactions for ferrielectric phases remains unresolved.

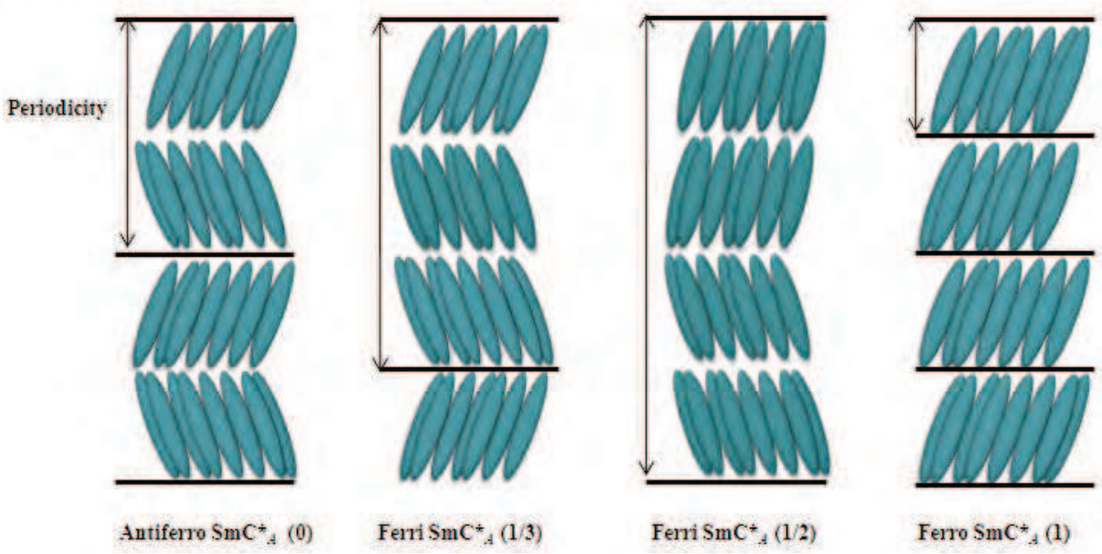

Fig. 1. Periodic structures of the frustrated smectic phases.

With respect to liquid-crystalline materials, ferrielectric phases have been observed for narrow temperature ranges of some highly chiral compounds. By decreasing the optical purity, a ferrielectric phase vanishes (Fukui et al., 1989; Gorecka et al., 2002). Nishiyama et al. reported a chiral twin molecule with wide temperatures of a ferrielectric phase (Nishiyama et al., 2001). In this case, the ferrielectric phase also disappears concomitantly with decreasing optical purity. Some mixtures of antiferroelectric chiral liquid crystals with highly chiral dopants of the same handedness were reported to exhibit ferrielectric phases with a range of 30 K (Jaradat at al., 2006). Asymmetric switching in a ferrielectric phase has been of interest in prospective devices (Jaradat et al., 2008, 2009). The molecular design for ferrielectric liquid crystals now constitutes an important issue not only because of their unusual phase structures but also because of their applications to optical devices.

Recently, we designed an asymmetric chiral dimer **(*R*)-I-(8,7)** and investigated its phase transition behaviour and electro-optical properties (Noji et al., 2009). The compound was found to exhibit ferrielectric phases with wide temperatures between antiferroelectric (Anti) and ferroelectric SmC* (Ferro) phases. Ferrielectric-like ordering was observed in a racemic mixture of the enantiomers. The appearance of the ferrielectric-like ordering in the racemic system without spontaneous polarization cannot be explained by any present physical model. Furthermore, its derivative **(*R*)-II-(8,7)** possessing an octyloxy tail instead of an octyl tail of **(*R*)-I-(8,7)** exhibits a direct transition from isotropic liquid to the ferrielectric phase (Noji & Yoshizawa, 2011).

We prepared a homologous series of liquid crystal oligomers and observed their physical properties. This report describes structure-property relations of liquid crystals and presents an origin for stabilizing the ferrielectric phases of the present chiral oligomeric system.

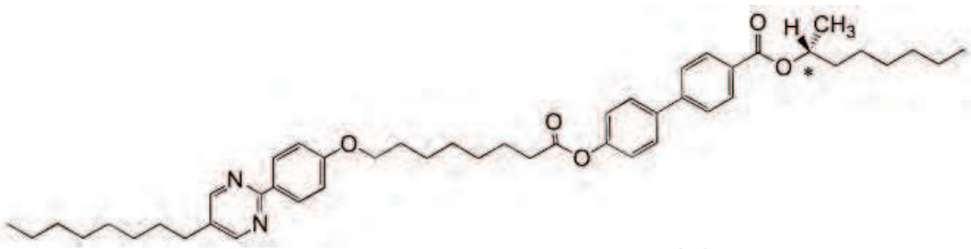

(*R*)-I-(8,7): Cry 83.8 Anti 85.2 Ferri-L 98.5 Ferri-H 111.8 Ferro 114.2 Iso

Fig. 2. Molecular structure and phase transition temperatures (°C) of **(*R*)-I-(8,7)**.

2. Experimental

2.1 Materials

For use in this study, 5-alkyl-2-(4-hydroxyphenyl)pyrimidine, 5-octyloxy-2-(4-hydroxyphenyl)pyridine, and 4-(4-hexyloxyphenyl)-1-(4-hydroxyphenyl)-2,3-difluorobenzene were purchased from Midori Kagaku Co. Ltd. The final compounds were prepared using a similar method to that used for **(*R*)-I-(8,7)**, as reported in our previous paper (Noji et al., 2009). The synthetic scheme is depicted in Fig. 3. Purification of each final product was conducted using column chromatography over silica gel (63–210 μm; Kanto Chemical Co. Inc.) using dichloromethane-ethyl acetate mixture as the eluent with subsequent recrystallization from ethanol. The purities of all final compounds were checked using HPLC (JAIGEL-1H column, LC9101; Japan Analytical Industry Co. Ltd.). Chloroform was used as eluent. Detection of products was achieved using UV irradiation (λ= 254 nm). Purities of the final compounds were also checked using elemental analysis (EA 1110; CE Instruments Ltd.). Infrared (IR) spectroscopy (FTS-30; Bio-Rad Laboratories Inc.) and proton nuclear magnetic resonance (^{1}H NMR) spectroscopy (JNM-ECA500; JEOL) elucidated the structure of each final product. Analytical data for the compounds are listed below.

(*R*)-1-Methylheptyl 4′-{6-[4-(5-octylpyrimidin-2-yl)phenyloxy]hexanoyloxy}biphenyl-4-carboxylate [(*R*)-I-(8,5)]

^{1}H NMR (500 MHz, solvent $CDCl_3$, standard TMS) δH/$_{ppm}$: 8.57 (s, 2H, Ar-**H**), 8.35 (d, 2H, Ar-**H**, *J* = 9.1 Hz), 8.10 (d, 2H, Ar-**H**, *J* = 8.3 Hz), 7.62 (d, 2H, Ar-**H**, *J* = 8.5 Hz), 7.60 (d, 2H, Ar-**H**, *J* = 8.6 Hz), 7.18 (d, 2H, Ar-**H**, *J* = 8.6 Hz), 6.99 (d, 2H, Ar-**H**, *J* = 8.8 Hz), 5.21-5.14 (m, 1H, -OC**H**(CH_3)-), 4.08 (t, 2H, -OC**H**$_2$-, *J* = 6.3 Hz), 2.65 (t, 2H, Ar-C**H**$_2$-, *J* = 7.4 Hz), 2.60 (t, 2H, -OCOC**H**$_2$-, *J* = 7.6 Hz), 1.93-1.85 (m, 4H, Ar-CH_2C**H**$_2$-, -OCH_2C**H**$_2$-), 1.79-1.58 (m, 6H, aliphatic-**H**), 1.43-1.28 (m, 18H, aliphatic-**H**), 1.35 (d, 3H, -OCH(C**H**$_3$)-, *J* = 6.3 Hz), 0.88 (t, 6H, -C**H**$_3$, *J* = 6.9 Hz); IR (KBr) ν_{max}/cm^{-1}: 2928, 2855 (C-H str.), 1761, 1706 (C=O str.), 1609, 1584 (C=C str.). HPLC: 100%. Anal. Calcd. for $C_{45}H_{58}N_2O_5$: C, 76.45% ; H, 8.27%; N, 3.96%. Found: C, 76.56%; H, 8.17%; N, 4.01%.

(*R*)-1-Methylheptyl 4′-{7-[4-(5-octylpyrimidin-2-yl)phenyloxy]heptanoyloxy}biphenyl-4-carboxylate [(*R*)-I-(8,6)]

^{1}H NMR (500 MHz, solvent $CDCl_3$, standard TMS) δH/$_{ppm}$: 8.57 (s, 2H, Ar-**H**), 8.35 (d, 2H, Ar-**H**, *J* = 8.7 Hz), 8.10 (d, 2H, Ar-**H**, *J* = 8.5 Hz), 7.62 (d, 2H, Ar-**H**, *J* = 8.4 Hz), 7.60 (d, 2H,

Ar-**H**, *J* = 8.5 Hz), 7.17 (d, 2H, Ar-**H**, *J* = 8.7 Hz), 6.99 (d, 2H, Ar-**H**, *J* = 9.1 Hz), 5.20-5.14 (m, 1H, -OC**H**(CH_3)-), 4.06 (t, 2H, -OC$\mathbf{H}_2$-, *J* = 6.4 Hz), 2.62 (t, 2H, Ar-C$\mathbf{H}_2$-, *J* = 7.5 Hz), 2.60 (t, 2H, -OCOC$\mathbf{H}_2$-, *J* = 7.7 Hz), 1.89-1.80 (m, 4H, Ar-CH_2C$\mathbf{H}_2$-, -OCH_2C$\mathbf{H}_2$-), 1.80-1.23 (m, 26H, aliphatic-**H**), 1.35 (d, 3H, -OCH(C$\mathbf{H}_3$)-, *J* = 6.3 Hz), 0.88 (t, 6H, -C$\mathbf{H}_3$, *J* = 6.9 Hz); IR (KBr) ν_{max}/cm^{-1}: 2948, 2852 (C-H str.), 1765, 1713 (C=O str.), 1607, 1582 (C=C str.). HPLC: 100%. Anal. Calcd. for $C_{46}H_{60}N_2O_5$: C, 76.63%; H, 8.39%; N, 3.89%. Found: C, 76.91%; H, 8.35%; N, 3.97%.

(*R*)-1-Methylheptyl 4′-{9-[4-(5-octylpyrimidin-2-yl)phenyloxy]nonanoyloxy}biphenyl-4-carboxylate [(*R*)-I-(8,8)]

^{1}H NMR (500 MHz, solvent $CDCl_3$, standard TMS) $\delta H/_{ppm}$: 8.57 (s, 2H, Ar-**H**), 8.34 (d, 2H, Ar-**H**, *J* = 9.0 Hz), 8.10 (d, 2H, Ar-**H**, *J* = 8.5 Hz), 7.62 (d, 2H, Ar-**H**, *J* = 8.5 Hz), 7.61 (d, 2H, Ar-H, *J* = 8.6 Hz), 7.18 (d, 2H, Ar-H, *J* = 8.7 Hz), 6.83 (d, 2H, Ar-H, *J* = 9.1 Hz), 5.20-5.14 (m, 1H, -OC**H**(CH_3)-), 4.04 (t, 2H, -OC$\mathbf{H}_2$-, *J* = 6.6 Hz), 2.60 (t, 4H, Ar-C$\mathbf{H}_2$-, OCOC$\mathbf{H}_2$-, *J* = 7.5 Hz), 1.86-1.72 (m, 5H, aliphatic-**H**), 1.67-1.59 (m, 3H, aliphatic-**H**), 1.52-1.28 (m, 26H, aliphatic-**H**), 1.35 (d, 3H, -OCH(C$\mathbf{H}_3$)-, *J* = 6.3 Hz), 0.88 (t, 6H, -C$\mathbf{H}_3$, *J* = 7.0 Hz); IR (KBr) ν_{max}/cm^{-1}: 2930, 2854 (C-H str.), 1767, 1710 (C=O str.), 1608, 1584 (C=C str.). HPLC: 100%. Anal. Calcd. for $C_{48}H_{64}N_2O_5$: C, 76.97%; H, 8.61%; N, 3.74%. Found: C, 77.01%; H, 8.59%; N, 3.75%.

(*R*)-1-Methylheptyl 4′-{6-[4-(5-dodecypyrimidin-2-yl)phenyloxy]hexanoyloxy}biphenyl-4-carboxylate [(*R*)-I-(12,5)]

^{1}H NMR (500 MHz, solvent $CDCl_3$, standard TMS) $\delta H/_{ppm}$: 8.57 (s, 2H, Ar-**H**), 8.36 (d, 2H, Ar-**H**, *J* = 8.8 Hz), 8.10 (d, 2H, Ar-**H**, *J* = 8.5 Hz), 7.63 (d, 2H, Ar-**H**, *J* = 8.4 Hz), 7.61 (d, 2H, Ar-**H**, *J* = 8.7 Hz), 7.18 (d, 2H, Ar-**H**, *J* = 8.6 Hz), 6.99 (d, 2H, Ar-**H**, *J* = 8.8 Hz), 5.20-5.14 (m, 1H, -OC**H**(CH_3)-), 4.08 (t, 2H, -OC$\mathbf{H}_2$-, *J* = 6.3 Hz), 2.65 (t, 2H, Ar-C$\mathbf{H}_2$-, *J* = 7.4 Hz), 2.60 (t, 2H, -OCOC$\mathbf{H}_2$-, *J* = 7.7 Hz), 1.93-1.85 (m, 4H, Ar-CH_2C$\mathbf{H}_2$-, -OCH_2C$\mathbf{H}_2$-), 1.79-1.58 (m, 6H, aliphatic-**H**), 1.45-1.26 (m, 24H, aliphatic-**H**), 1.35 (d, 3H, -OCH(C$\mathbf{H}_3$)-, *J* = 6.3 Hz), 0.88 (t, 6H, -C$\mathbf{H}_3$, *J* = 6.9 Hz); IR (KBr) ν_{max}/cm^{-1}: 2921, 2850 (C-H str.), 1760, 1709 (C=O str.), 1608, 1585 (C=C str.). HPLC: 100%. Anal. Calcd. for $C_{50}H_{68}N_2O_5$: C, 77.13%; H, 8.72%; N, 3.67%. Found: C, 77.13%; H, 8.73%; N, 3.71%.

(*R*)-1-Methylheptyl 4′-{8-[4-(5-octyloxypyridin-2-yl)phenyloxy]octanoyloxy}biphenyl-4-carboxylate [(*R*)-III-(8,7)]

^{1}H NMR (500 MHz, solvent $CDCl_3$, standard TMS) $\delta H/_{ppm}$: 8.33 (d, 1H, Ar-**H**, *J* = 2.9 Hz), 8.10 (d, 2H, Ar-**H**, *J* = 8.4 Hz), 7.85 (d, 2H, Ar-**H**, *J* = 9.0 Hz), 7.62 (d, 2H, Ar-**H**, *J* = 8.3 Hz), 7.61 (d, 2H, Ar-**H**, *J* = 8.7 Hz), 7.57 (d, 1H, Ar-**H**, *J* = 8.7 Hz), 7.22 (dd, 1H, Ar-**H**, *J* = 8.9 Hz, *J* = 3.0 Hz), 6.97 (d, 2H, Ar-**H**, *J* = 9.0 Hz), 5.20-5.14 (m, 1H, -OC**H**(CH_3)-), 4.03 (t, 2H, -OC$\mathbf{H}_2$-, *J* = 5.7 Hz), 2.60 (t, 2H, -OCOC$\mathbf{H}_2$-, *J* = 7.4 Hz), 1.86-1.72 (m, 8H, aliphatic-**H**), 1.65-1.29 (m, 24H, aliphatic-**H**), 1.35 (d, 3H, -OCH(C$\mathbf{H}_3$)-, *J* = 6.2 Hz), 0.89 (t, 3H, -C$\mathbf{H}_3$, *J* = 6.6 Hz), 0.88 (t, 3H, -C$\mathbf{H}_3$, *J* = 6.9 Hz); IR (KBr) ν_{max}/cm^{-1}: 2924, 2854 (C-H str.), 1754, 1714 (C=O str.), 1609, 1582 (C=C str.). HPLC: 100%. Anal. Calcd. for $C_{48}H_{63}NO_6$: C, 76.87%; H, 8.47%; N, 1.87%. Found: C, 77.38%; H, 8.47%; N, 1.86%.

(*R*)-1-Methylheptyl 4′-{8-[4-(4-(4-hexylphenyl)-2,3-difluoro phenyl)]phenyloxy} octanoyloxy}biphenyl-4-carboxylate [(*R*)-IV-(6,7)]

^{1}H NMR (500 MHz, solvent $CDCl_3$, standard TMS) $\delta H/_{ppm}$: 8.09 (d, 2H, Ar-**H**, *J* = 8.1 Hz), 7.62 (d, 2H, Ar-**H**, *J* = 8.6 Hz), 7.61 (d, 2H, Ar-**H**, *J* = 8.6 Hz), 7.53-7.49 (m, 4H, Ar-**H**), 7.28 (d,

2H, Ar-**H**, *J* = 8.1 Hz), 7.23-7.21 (m, 2H, Ar-**H**), 7.18 (d, 2H, Ar-**H**, *J* = 8.6 Hz), 6.99 (d, 2H, Ar-**H**, *J* = 8.6 Hz), 5.20-5.14 (m, 1H, -OC**H**(CH_3)-), 4.03 (t, 2H, -OC**H**$_2$-, *J* = 5.6 Hz), 2.66 (t, 2H, Ar-C**H**$_2$-, *J* = 8.0 Hz), 2.60 (t, 2H, -OCOC**H**$_2$-, *J* = 7.5 Hz), 1.87-1.28 (m, 28H, aliphatic-**H**), 1.35 (d, 3H, -OCH(C**H**$_3$)-, *J* = 6.3 Hz), 0.90 (t, 3H, -C**H**$_3$, *J* = 7.2 Hz), 0.88 (t, 3H, -C**H**$_3$, *J* = 6.9 Hz); IR (KBr) ν_{max}/cm^{-1}: 2931, 2855 (C-H str.), 1754, 1718 (C=O str.), 1613, 1527 (C=C str.). HPLC: 100%. Anal. Calcd. for $C_{53}H_{62}F_2O_5$: C, 77.91%; H, 7.65%. Found: C, 78.57%; H, 7.69%.

(*S*)-4-[4-(2-Methyloctanoyl)phenyl]phenyl 8-[4-(5-octylpyrimidin-2-yl)phenyloxy] octanoate [(*S*)-V-(8,7)]

^{1}H NMR (500 MHz, solvent $CDCl_3$, standard TMS) $\delta H/_{ppm}$: 8.57 (s, 2H, Ar-**H**), 8.35 (d, 2H, Ar-**H**, *J* = 8.7 Hz), 8.02 (d, 2H, Ar-**H**, *J* = 8.5 Hz), 7.66 (d, 2H, Ar-**H**, *J* = 8.5 Hz), 7.62 (d, 2H, Ar-**H**, *J* = 8.6 Hz), 7.19 (d, 2H, Ar-**H**, *J* = 8.6 Hz), 6.98 (d, 2H, Ar-**H**, *J* = 8.9 Hz), 4.04 (t, 2H, -OC**H**$_2$-, *J* = 6.6 Hz), 3.52-3.45 (m, 1H, -COC**H**(CH_3)-), 2.60 (t, 2H, Ar-C**H**$_2$-, *J* = 7.5 Hz), 2.59 (t, 2H, -OCOC**H**$_2$-, *J* = 7.6 Hz), 1.87-1.77 (m, 6H, aliphatic-**H**), 1.68-1.24 (m, 26H, aliphatic-**H**), 1.21 (d, 3H, -OCH(C**H**$_3$)-, *J* = 6.9 Hz), 0.88 (t, 6H, -C**H**$_3$, *J* = 6.9 Hz); IR (KBr) ν_{max}/cm^{-1}: 2925, 22851 (C-H str.), 1748, 1674 (C=O str.), 1586, 1542 (C=C str.). HPLC: 100%. Anal. Calcd. for $C_{47}H_{62}N_2O_4$: C, 78.51%; H, 8.69%; N, 3.90%. Found: C, 78.80%; H, 8.65%; N, 3.93%.

2.2 Physical properties

The initial phase assignments and corresponding transition temperatures for the final products were determined using polarized optical microscopy (POM) with a polarizing microscope (Optiphot-pol; Nikon Corp.) equipped with a hot stage (FP82; Mettler Inst. Corp.) and a control processor (FP80; Mettler Inst. Corp.). The heating and cooling rates were 5 °C min^{-1}. Temperatures and enthalpies of transition were investigated using differential scanning calorimetry (DSC, DSC6200; Seiko Instruments Inc.). The materials were studied at a scanning rate of 5 °C min^{-1} after encapsulation in aluminium pans. The X-ray diffraction (XRD) patterns of the powder samples on cooling processes were obtained using a real-time X-ray diffractometer (D8 Discover; Bruker AXS GmbH). A sample was put on a convex lens, which was placed in a custom-made temperature stabilized holder (stability within ±0.1 °C). The textural observations were conducted using polarized light microscopy with a CCD camera. The X-ray apparatus was equipped with a cross-coupled Göbel mirror on a platform system with a two-dimensional position-sensitive proportional counter (PSPC) detector (HI-Star; Bruker AXS GmbH). X-rays were generated at 40 kV and 40 mA; a parallel Cu Kα X-ray beam was used to irradiate the sample.

Electro-optical studies were conducted using commercially available evaluation cells (E. H. C. Co., Ltd., Japan). The inner surfaces had been coated with a polyimide aligning agent and had been buffed unidirectionally. The cells were made with 5 μm spacings. Switching current and optical tilt angle across the temperatures of tilted smectic phases were measured using standard electro-optic techniques (Goodby et al., 1991). The optical tilt angle was determined by finding the extinction direction when an electric field was applied to the specimen in increasing or decreasing steps. A Kikusui Electric Regulated DC Power Supply was used to supply the d.c. field.

3. Results and discussion

We prepared a homologous series of the chiral dimesogenic compound and investigated the effects of terminal chain, central spacer, core structure, and chiral moiety of the chiral dimesogenic compound on appearance of the ferrielectric phase.

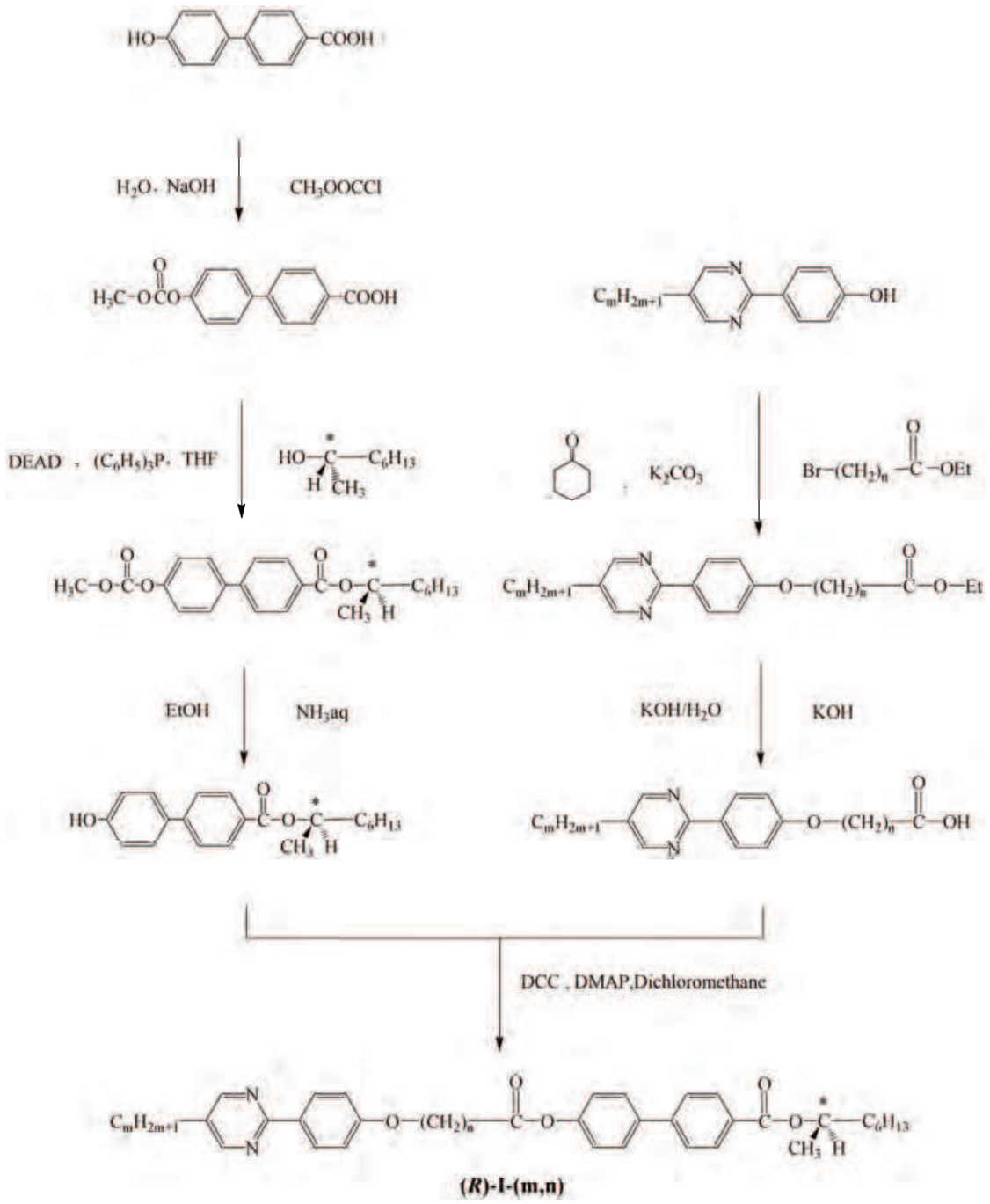

Fig. 3. Synthetic scheme of compound **(*R*)-I-(m,n)**.

3.1 Effects of the central spacer

We investigated effects of parity of the central spacer of the compounds on the phase transition behaviour. Transition temperatures and associated entropy changes, $\Delta S/R$ for **(*R*)-I-(m,n)** are listed in Table 1. The parity of the space is calculated as n (methylene number) plus 3 (one carbon and two oxygens). Compounds **(*R*)-I-(8,5)** and **(*R*)-I-(8,7)** with the even-

numbered spacer exhibited Ferro, Ferri-H, Ferri-L, and Anti phases, whereas compounds **(*R*)-I-(8,6)** and **(*R*)-I-(8,8)** with the odd-numbered spacer showed Ferro, Ferri-L, Anti, chiral smectic I (SmI*), and unidentified SmX phases. Furthermore, compound **(*R*)-I-(8,6)** showed a SmC^*_α phase. The ferrielectric phases were distinguishable from the antiferroelectric or ferroelectric phase under a polarized microscope because the characteristic texture with constant motion as domains form, coalesce, and disappear was observed, as reported for monomeric (Goodby et al., 1992) and dimeric materials (Nishiyama et al., 2001).

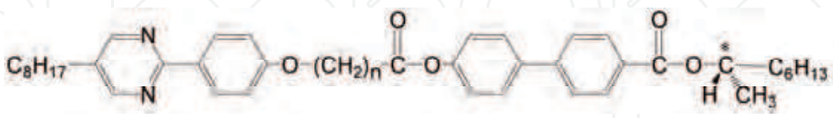

(*R*)-I-(8,n)

n	Cr	SmX	SmI*	Anti	Ferri-L	Ferri-H	Ferro	SmC^*_α	Iso
5	• 82.5			[•78.8] (0.55)	• 114.3 (-)	• 126.5 (-)	• 130.7 (5.37)		•
6	• 71.6	[• 50.8 (0.49)	• 65.6 (-)	• 69.6] (-)	• 73.6 (-)		• 83.0 (-)	• 85.0 (5.11)	•
7	• 83.8			•85.2 (0.76)	• 98.5 (-)	• 111.8 (-)	• 114.2 (6.34)		•
8	• 78.5	[• 69.3 (0.36)	• 72.0 (0.24)	• 75.7 (-)	• 76.3] (-)		• 83.1 (6.71)		•

Table 1. Transition temperatures (°C) and $\Delta S/R$ (in parentheses) for **(*R*)-I-(8,n)**. Square brackets represent a monotropic transition.

Figure 4 depicts optical textures of SmC^*_α, Ferro, Ferri-L, Anti, SmI*, and SmX phases of **(*R*)-I-(8,6)**. The typical fan texture in planar alignment regions and dark texture attributable to the short pitch helical structure in homeotropic regions were observed in the SmC^*_α phase [Fig. 4(a)]. In the Ferri-L phase [Fig. 4(c)], a characteristic texture with vigorous constant movement was observed. The constant motion in the Ferr-L phase was weaker than that in Ferri-H phase. Upon cooling to the Anti phase, the homeotropic alignment exhibited a dark texture and the constant movement was no longer present [Fig. 4(d)].

Figure 5 portrays a cooling thermogram of **(*R*)-I-(8,6)**. Neither Ferro-to-Ferri-L nor the Ferri-L-to-Anti transition accompanied enthalpy change. In contrast, the Ferri-L-to-Anti transition of **(*R*)-I-(8,7)** showed clear enthalpy change.

Odd–even effects were observed not only for the phase sequence but also for the Iso-Ferro (or SmC^*_α) phase transition temperature. The transition temperatures of the even-numbered series are higher than those of the odd-numbered series. However, it is noteworthy that such an odd–even effect was not observed for the associated entropy changes. Typical liquid crystal dimers show marked odd–even effects not only on the transition temperature but also on the associated entropy changes. The effects on the entropy changes are interpreted as follows (Imrie & Luckhurst, 1998). In the isotropic phase, approximately half the conformers of an even-membered dimer are essentially linear; for an odd–membered dimer, only 10% are linear. A synergy exists between conformation and orientational order. Therefore, many of the bent conformers are converted to a linear form at the transition to the nematic phase for even-membered dimers, which enhances the orientational order of the nematic phase, engendering a larger nematic–isotropic entropy than would be expected for a monomer. For odd-membered dimers, however, the difference in free energy between the bent and linear conformers is such that the orientational order of the nematic phase is insufficient to convert

bent into linear conformers. Consequently, the orientational order is not enhanced and a smaller nematic-isotropic entropy is expected. In the present system, compound **(*R*)-I-(8,8)** with an odd-numbered spacer has larger entropy change at the Iso-Ferro transition than compound **(*R*)-I-(8,7)** with an even-numbered spacer. The unusually larger entropy change for the odd-membered series reflects that not only the even-membered compounds but also the odd-membered compounds exhibit the conformational change from bent to linear at the Iso-to-Ferro (or SmC^*_α) transition. Therefore, both even-membered and odd-membered compounds exist as linear conformers in their respective Ferro and Ferri phases.

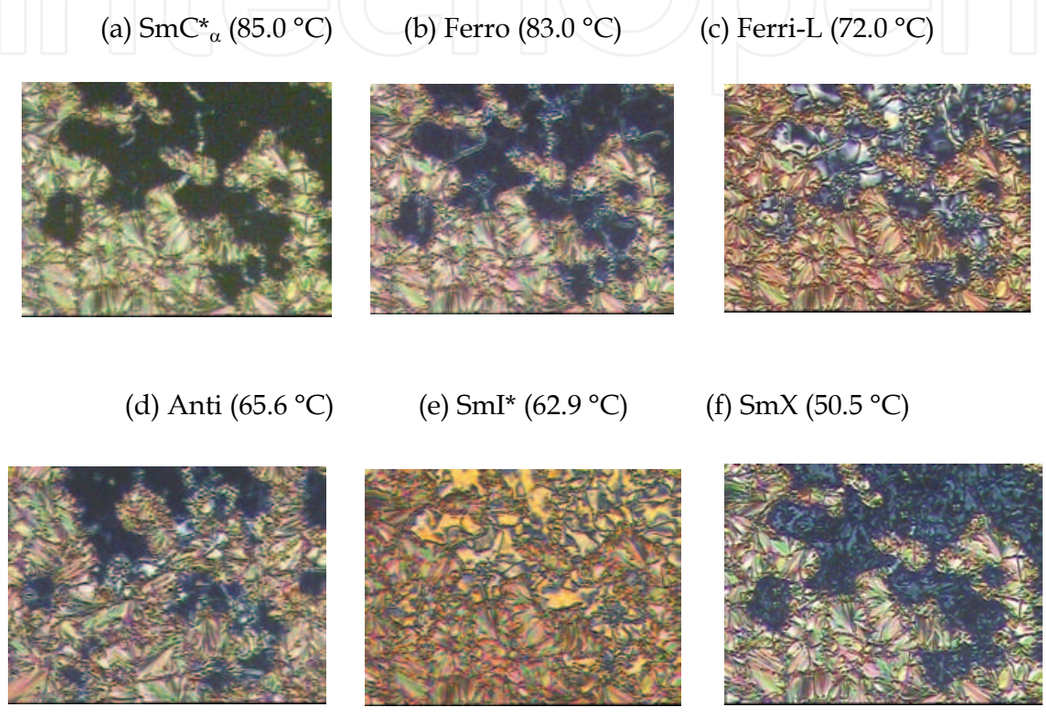

Fig. 4. Optical textures of **(*R*)-I-(8,6)** on a glass with a cover glass.

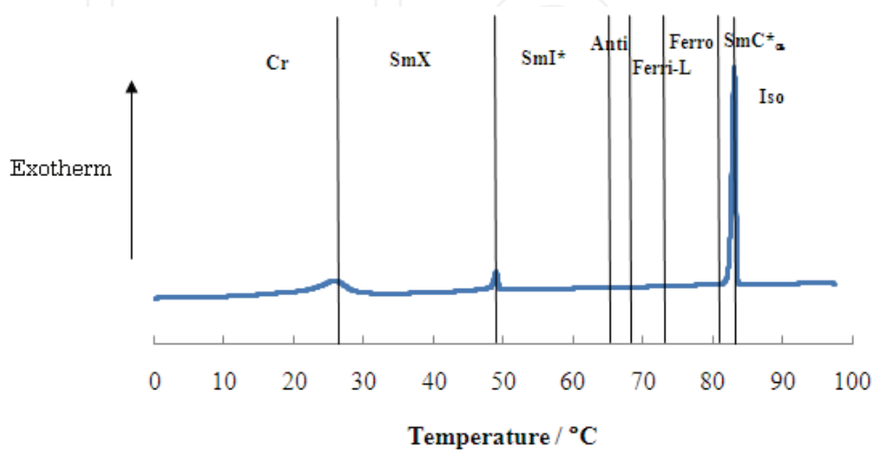

Fig. 5. Cooling DSC thermogram of **(*R*)-I-(8,6)** at a scanning rate of 5 °C min^{-1}.

Ferrielectric properties in the Ferri-L phase of compound **(*R*)-I-(8,6)** were studied using measurements of the apparent tilt angle as a function of the applied voltage. Figure 6(a) presents the applied voltage dependence of the apparent tilt angle in the Ferri-L phase. When the applied voltage is increased, the apparent tilt angle increases and reaches a saturated value corresponding to the electrically induced ferroelectric ordering via characteristic multi-step change (Nishiyama et al., 2001). Figure 6(b) portrays the temperature dependence of a saturated tilt angle corresponding to the electrically induced ferroelectric state with an electric field of 8 V μm^{-1}. The tilt angle increases concomitantly with decreasing temperature in the Ferro and Ferri-L phases.

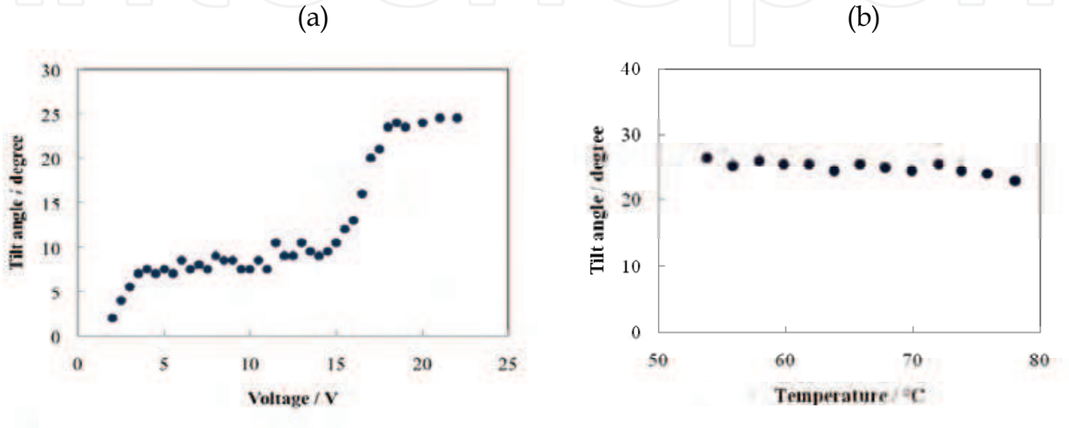

Fig. 6. (a) Applied voltage dependence of the apparent tilt angle in the Ferri-L phase of compound **(*R*)-I-(8,6)** at 71 °C. The cell gap was 5 μm. (b) The saturated tilt angle as a function of temperature, corresponding to the electrically induced ferroelectric state of **(*R*)-I-(8,6)** with an electric field of 8 V μm^{-1}. The cell gap was 5 μm.

Layer spacings in the Ferro and Ferri-L phases of compound **(*R*)-I-(8,6)** were investigated using XRD measurements. A sharp peak was observed in the small angle region. Layer spacings corresponding to the peak are 44.6 Å in the Ferro phase and 44.1 Å in the Ferri-L phase. The molecular lengths were obtained from MOPAC as about 46 Å for a bent conformer and 44 Å for a linear conformer. According to the larger transition entropy at the Iso-to-SmC*$_\alpha$ as discussed above, we assume that compound **(*R*)-I-(8,6)** forms a linear conformation in the Ferro and Ferri phases. The Ferri-L phase of compound **(*R*)-I-(8,6)** is thought to have a monolayer structure, as does that of **(*R*)-I-(8,7)**.

Figure 7 shows the binary phase diagram between compounds **(*R*)-I-(8,6)** and **(*R*)-I-(8,7)**. The SmC*$_\alpha$ phase disappears as increasing content of compound **(*R*)-I-(8,7)**. It is particularly interesting that the Ferro phase disappears between 50–75 mol% of compound **(*R*)-I-(8,7)**, and the direct transition from Iso to Ferri-H was observed. The Ferri-L phase of both compounds proved to be miscible across the full composition range. Therefore, the Ferri-L phase of compound **(*R*)-I-(8,6)** has the same structure as that of compound **(*R*)-I-(8,7)**.

To summarize the effects of the central spacer on the appearance of the ferrielectric phases of the chiral dimesogenic compound, the compounds possessing an even-numbered spacer show both Ferri-H and Ferri-L phases with a wide temperature range, although the compounds possessing an odd-numbered spacer show only a Ferri-L phase. Furthermore, no significant difference was found in the electro-optical properties in the Ferri-L phase

between even– and odd-membered series. Both even– and odd-membered compounds have a monolayer structure in the smectic phases. Unusual entropy change observed at the Iso-Ferro or Iso-SmC*$_\alpha$ of the odd-membered compounds indicates that they exist as a linear conformer in the Ferro and Ferri-L phases.

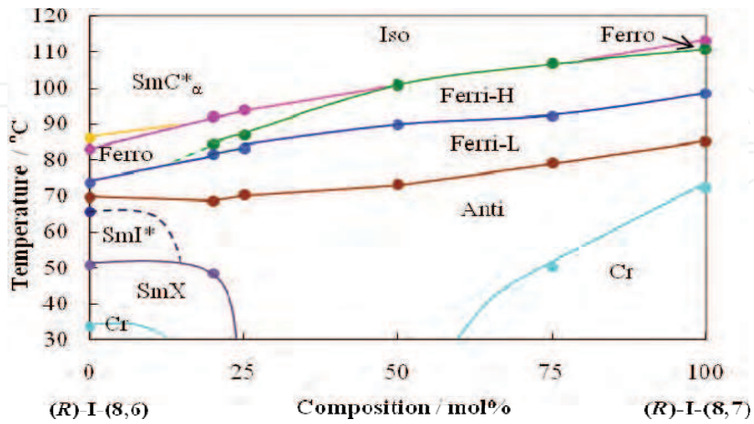

Fig. 7. Binary phase diagram between compounds **(*R*)-I-(8,6)** and **(*R*)-I-(8,7)**.

3.2 Effects of the terminal chain

We prepared compound **(*R*)-I-(12,5)** possessing a decyl chain instead of an octyl chain of compound **(*R*)-I-(8,5)** and investigated its physical properties. Figure 8 depicts its molecular structure and transition properties. Compound **(*R*)-I-(12,5)** shows Ferro, Ferri-H, Ferri-L, and Anti phases, as does the corresponding compound **(*R*)-I-(8,5)**. In addition to the phases, an unidentifed SmX phase was observed for compound **(*R*)-I-(12,5)**. The Iso-to-N and Ferri-L-to-Anti phase transition temperatures are almost identical among them. However, compound **(*R*)-I-(12,5)** shows lower transition temperatures for the Ferro-to-Ferri-H and Ferri-H-to-Ferri-L phase transition than compound **(*R*)-I-(8,5)** does. Increasing the terminal chain length destabilizes both Ferri-H and Ferri-L phases. The terminal alkyl chain is thought to play an important role in the interlayer interaction stabilizing the ferrielectric phases.

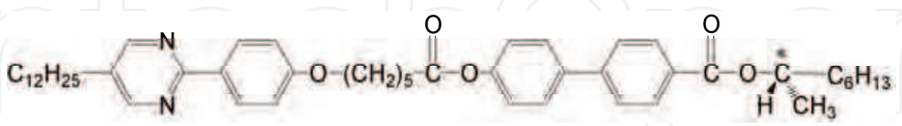

(*R*)-I-(12,5): Cry 76.6 [SmX 60.8(0.36)] Anti 79.6(-) Ferri-L 87.1(-) Ferri-H 105.3(-) Ferro128.4(5.93) Iso

Fig. 8. Molecular structure, transition temperatures (°C) and $\Delta S/R$ for **(*R*)-I-(12,5)**.

Recent reports describe that the octyloxy derivative **(*R*)-II-(8,7)** exhibits a direct Iso-to-Ferri-H transition (Noji & Yoshizawa, 2011). Figure 9 shows the molecular structure and the transition properties. Compound **(*R*)-II-(8,7)** shows Ferro, Ferri-H, Ferri-L, Anti, and SmI* phases. The temperature range of the enantiotropic ferrielectric phases was about 28 K. According to a binary phase diagram between compounds **(*R*)-II-(8,7)** and **(*R*)-I-(8,7)**, both Ferri-H and Ferri-L phases of compound **(*R*)-II-(8,7)** present a similar structure to those of compound **(*R*)-I-(8,7)**. Comparing compound **(*R*)-II-(8,7)** with **(*R*)-I-(8,7)**, the alkoxy tail

substituted to the pyrimidine ring stabilizes the Ferri-L phase much more than the Ferri-H phase.

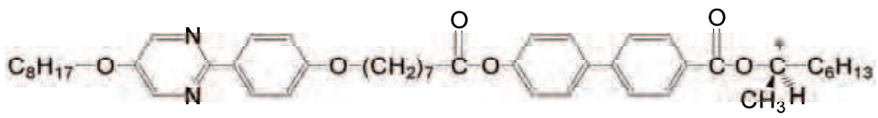

(*R*)-II-(8,7): Cry 105.9 [SmI 92.0(4.77) Anti 95.8(0.64)]Ferri-L 126.0(-) Ferri-H 134.3(7.31) Iso

Fig. 9. Molecular structure, transition temperatures (°C) and $\Delta S/R$ for **(*R*)-II-(8,7)** (Noji & Yoshizawa, 2011).

The wide temperature ranges of the ferrielectric phases enable observation of the switching current in the Ferri-H phase [Fig. 10(a)] and that in the Ferri-L phase [Fig. 10(b)].

(a) Ferri-H phase (b) Ferri-L phase

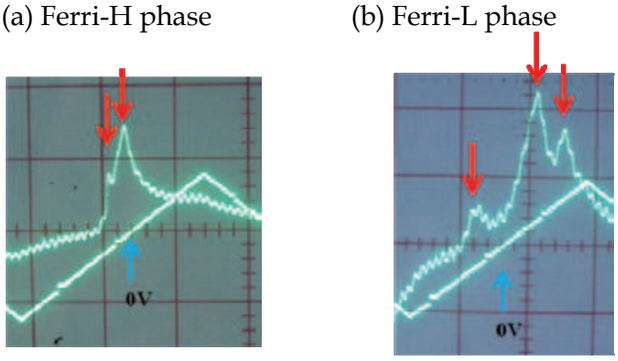

Fig. 10. Electrical response in switching current under triangular waves in (a) the Ferri-H phase at 130 °C and (b) the Ferri-L phase at 110 °C of compound **(*R*)-II-(8,7)**. The cell gap was 5 μm. The voltage was changed from -50 V to +50 V at 1 Hz (Noji & Yoshizawa, 2011).

Two asymmetric peaks in the Ferri-H phase suggest that switching between two ferroelectric states occurs via one intermediate state. Figure 11 shows a schematic model for the switching behaviour assuming that the intermediate state has four-layer periodicity.

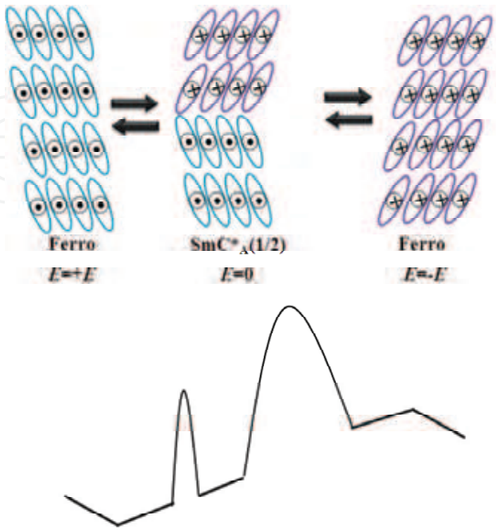

Fig. 11. Schematic model for electrical switching behaviour in the Ferri-H phase.

With respect to the Ferri-L phase, its three asymmetric peaks suggest that switching between two ferroelectric states occurs via two intermediate states. Figure 12 shows a model for the switching behaviour assuming that the intermediate state has three-layer periodicity.

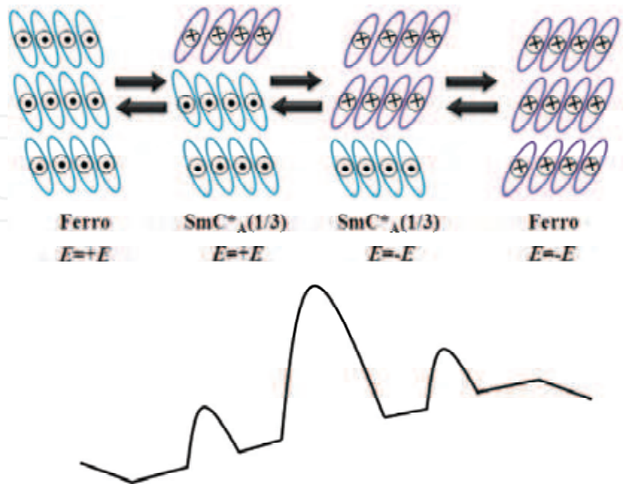

Fig. 12. Schematic model for electrical switching behaviour in the Ferri-L phase.

Asymmetric switching was observed in both the Ferri-H and Ferri-L phases. We have no explanation for the asymmetric switching. It is possible that the Ferri-H and Ferri-L phases have a more complex periodicity.

A ferrielectric phase normally arises at the lower temperature end of the ferroelectric smectic C phase. A direct transition is unusual. The introduction of the alkoxy tail to the chiral oligomeric system produces marked stability of the ferrielectric phases.

3.3 Effects of the mesogenic core structure

We introduced a phenylpyridine core or a 2,3-difluro-1,4-diphenylbenzene core into the chiral oligomeric system instead of a phenylpyrimidine core and investigated the liquid-crystalline properties. Figure 13 shows the molecular structure and phase transition properties of compound **(*R*)-III-(8,7)** possessing a phenylpyridine core with greater tilt ability than that of a phenylpyridine core.

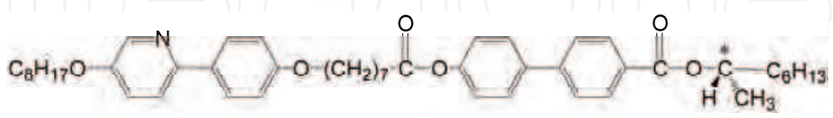

(*R*)-III-(8,7): Cry 108.7 Anti 122.7(1.72) Ferri-L 125.0(-)Ferri-H 134.7 Ferro 139.3(7.24) Iso

Fig. 13. Molecular structure, transition temperatures (°C) and $\Delta S/R$ for **(*R*)-III-(8,7)**.

Figure 14 depicts optical textures of Ferro, Ferri-H, Ferri-L, and Anti phases of **(*R*)-III-(8,7)**. Ferro-to-Ferri-H and Ferri-H-to-Ferri-L transition temperatures of compound **(*R*)-III-(8,7)** are almost identical as those of compound **(*R*)-II-(8,7)**, suggesting that no significant difference exists in stability of the ferrielectric phases between those compounds. However, the Ferro phase appears in compound **(*R*)-III-(8,7)**. Furthermore, the Ferri-L-to-Anti phase transition temperature of compound **(*R*)-III-(8,7)** is much higher than that of compound **(*R*)-**

II-(8,7). Therefore, the temperature ranges of the ferrielectric phases of compound **(*R*)-III-(8,7)** are narrower than that of compound **(*R*)-II-(8,7)**.

(a) Ferro (130.7 °C) (b) Ferri-H (130.0 °C)

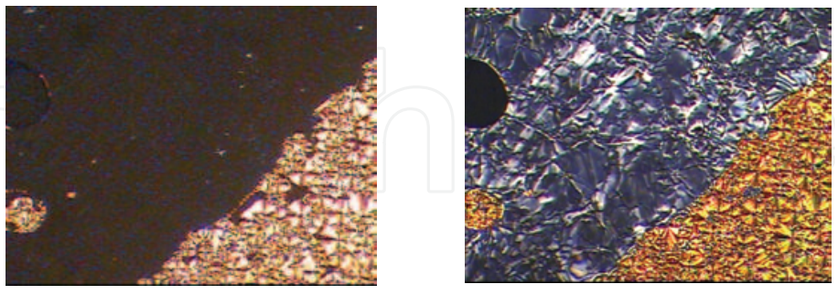

(c) Ferri-L (123.9 °C) (d) Anti (83.3 °C)

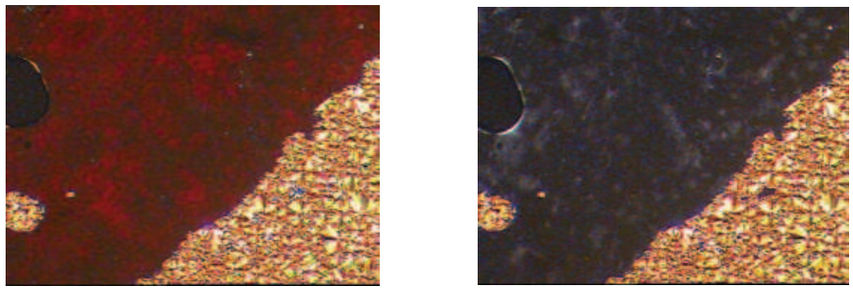

Fig. 14. Optical textures of **(*R*)-III-(8,7)** on a glass with a cover glass.

Figure 15 shows molecular structure and phase transition properties of compound **(*R*)-IV-(6,7)** possessing a 2,3-difluro-1,4-diphenylbenzene core that stabilizes a nematic phase.

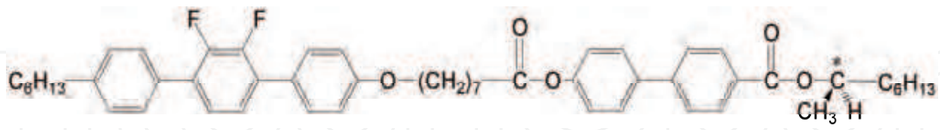

(*R*)-IV-(6,7): Cry 108.2 [SmX 79.5 (1.36) Anti 95.3 (-)] Ferro 111.0 (-) SmA 156.9 (4.66) Iso

Fig. 15. Molecular structure, transition temperatures (°C) and $\Delta S/R$ for **(*R*)-IV-(6,7)**.

Compound **(*R*)-IV-(6,7)** exhibited smectic A, Ferro, Anti, and unidentified SmX phases. No ferrielectric phase was observed.

A phenylpyridine core having larger tilting ability than a phenylpyrimidine core enhances the stability of the Ferro and Anti phases; however, it does not affect that of the ferrielectric phases. Intermolecular tilting interactions between adjacent mesogenic units make no large contribution to the stability of the ferrielectric phases. A 2,3-difluro-1,4-diphenylbenzene core making the mesogenic units to align along the director induces a SmA phase but eliminates both of the Ferri-H and Ferri-L phases. A phase sequence of

SmA-Ferro-Ferri is often observed for some monomeric chiral compounds. However, the ferrielectric phases of the present chiral oligomeric system are thought unlikely to coexist with a SmA phase.

3.4 Effects of chirality

The appearance of ferrielectric phases is known to be highly dependent on the optical purity of the system. Actually, ferrielectric phases are seen only in high enantiomer excess areas. We reported that ferrielectric-like ordering was observed in a racemic mixture of **(*R*)-I-(8,7)** and its enantiomer (Noji at al., 2009). Figure 16 depicts a binary phase diagram for mixtures of **(*S*)-I-(8,7)** and **(*R*)-I-(8,7)**. Stabilities of both the ferroelectric and antiferroelectric phases were independent of the optical purity. The Ferro-to-Ferri-H transition temperature decreases concomitantly with decreasing optical purity, although the Ferri-H-to-Ferri-L transition temperature increases slightly and then decreases concomitantly with decreasing optical purity. Surprisingly, the Ferri-L phase does not disappear with decreasing optical purity close to 0% enantiomer excess. The results indicate that a ferrielectric phase appears in a system with a low degree of chirality, and ferrielectric-like ordering exists in the racemic mixture.

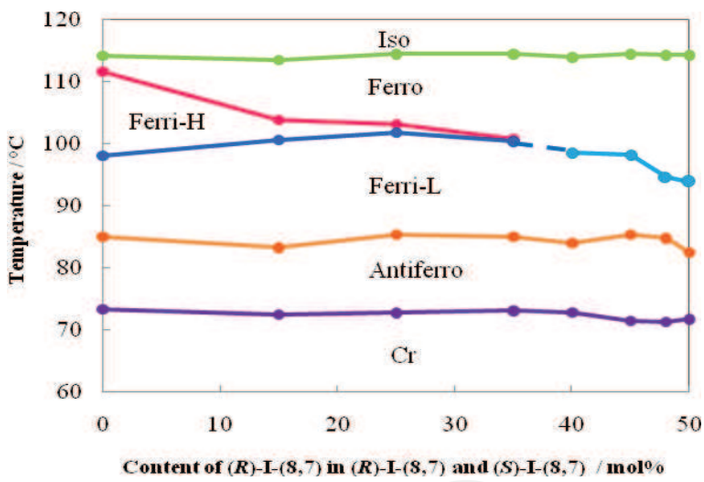

Fig. 16. Binary phase diagram for mixtures of **(*S*)-I-(8,7)** and **(*R*)-I-(8,7)** (Noji et al., 2009).

We prepared compound **(*S*)-V-(8,7)** possessing a (*S*)-2-methylalkanoyl group as the chiral structure. A ferroelectric liquid crystal possessing a 2-methylalkanoyl group gives usually larger spontaneous polarization in the ferroelectric SmC* phase than that possessing a 1-methylheptyl carboxylate group (Yoshizawa et al. 1989). Therefore, compound **(*S*)-V-(8,7)** is thought to have a higher degree of chirality than **(*R*)-I-(8,7)** has. Figure 17 presents the molecular structure and phase transition properties of compound **(*S*)-V-(8,7)**.

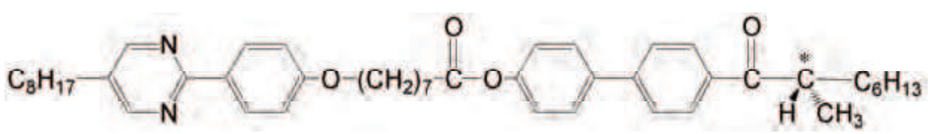

(*S*)-V-(8,7): Cry 95.1 [SmX 91.8 (1.09)] Anti 109.5 (-) Ferro 115.5 (6.10) Iso

Fig. 17. Molecular structure, transition temperatures (°C) and $\Delta S/R$ for **(*S*)-V-(8,7)**.

Compound **(*S*)-V-(8,7)** exhibited Ferro and Anti phases without accompanying any ferrielectric phase. Comparing transition temperatures of compound **(*S*)-V-(8,7)** with those of compound **(*R*)-I-(8,7)**, the Iso-to-Ferro transition temperature of **(*S*)-V-(8,7)** is almost identical to that of **(*R*)-I-(8,7)**, whereas the Ferro-to-Anti transition temperature of **(*S*)-V-(8,7)** is much higher than the Ferri-L-to-Anti transition temperature of **(*R*)-I-(8,7)**. The disappearance of a ferrielectric phase for **(*S*)-V-(8,7)** is attributed to the higher stability of the Anti phase of **(*S*)-V-(8,7)**. Furthermore, significant difference exhists in the molecular shape between compounds **(*R*)-I-(8,7)** and **(*S*)-V-(8,7)**. Figure 18 presents MOPAC models for those compounds. The 2-methyloctanoyl group has a bent structure because of the keto carbon, as presented in Fig. 18(b). The inclined structure between the core and the alkyl chain disturbs the interlayer interaction related to the appearance of the ferrielectric phase.

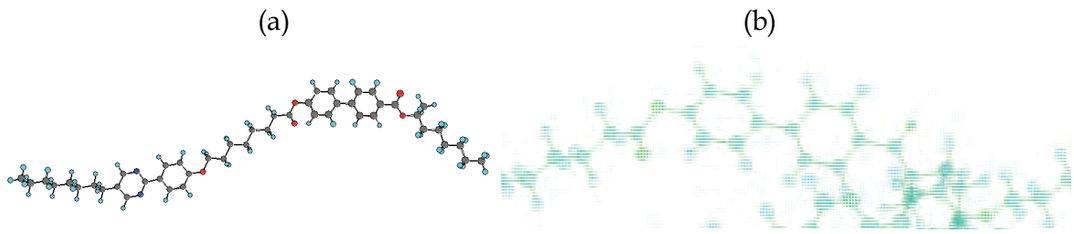

Fig. 18. MOPAC models for (a) **(*R*)-I-(8,7)** and (b) **(*S*)-V-(8,7)**.

3.5 Origin for stabilizing the ferrielectric phases

Electrical response studies of compound **(*R*)-II-(8,7)** reveal that the Ferri-H and Ferri-L phases respectively have a four-layer periodicity as SmC*$_A$(1/2) and a thee-layer periodicity as SmC*$_A$(1/3). We discuss the origin for stabilizing the ferrielectric phases in terms of preorganization and interlayer interaction, and show molecular organization models for the ferrielectric phases.

3.5.1 Preorganized effects

According to the XRD measurements, both the Ferri-H and Ferri-L phases have a monolayer structure. Comparison of tilt angles determined by POM with those determined by XRD of **(*R*)-I-(8,7)** reveals that the tilt of the mesogenic units is greater than that of the long axis (Noji et al., 2009). The dimesogenic system has an inherent tilt within the molecule. The two mesogenic units are connected via a central spacer. Assuming that all *trans* conformation for the spacer, then compounds **(*R*)-I-(8,n)** possessing an even-numbered spacer can form a linear conformation with two coparallel mesogenic units, as presented in Fig. 19(a). Optical tilt angles in the Ferro, Ferri-H, Ferri-L, and Anti phases of these compounds are attributed to the tilt of the mesogenic units with respect to the layer normal. However, compounds **(*R*)-I-(8,n)** possessing an odd-numbered spacer are thought to form a bent conformation in which two mesogenic units are inclined with respect to each other. The unusual large entropy change at the Iso-Ferro (or SmC*) suggests that the conformational change from bent to linear occurs at the phase transition. In the Ferri-L phase of the odd-members, the molecules are thought to exist as a linear conformer in which two mesogenic units are coparallel, as presented in Fig. 19(b). Therefore, both even– and odd-membered compounds have two mesogenic units tilted

with respect to the long axis in their smectic phases. The inherent tilt within a single molecule can stabilize the ferrielectric phases. However, it might disturb the appearance of a smectic A phase for these ferrielectric compounds.

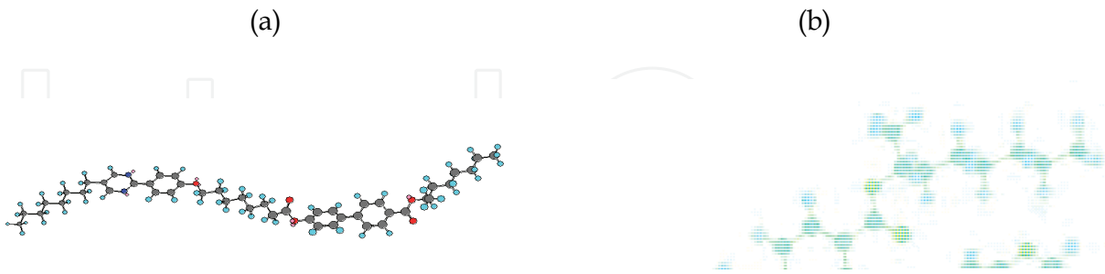

Fig. 19. Linear conformations for (a) the even-member **(*R*)-I-(8,7)** and (b) the odd-member **(*R*)-I-(8,6)**.

3.5.2 Interlayer interactions

It is generally accepted that the appearance of a ferrielectric phase is explained in terms of macroscopic chirality, i.e. helicity or spontaneous polarization. In this system, the Ferri-H phase is destabilized by decreasing optical purity. However, the macroscopic chirality does not affect the stability of the Ferri-L phase. Another model is necessary to explain the stabilization of the ferrielectric phase. We infer interlayer interactions among the preorganized molecules in adjacent layers via chiral recognition to discuss the stability of the Ferri-L phase. Interlayer interactions are known to govern tilt– and helical-correlation between molecules in adjacent layers (Yoshizawa et al., 1995; Yoshizawa & Nishiyama, 1995). Two molecular arrangements for the chiral interaction exist as presented in Fig. 20. One is a parallel twin ordering in which two oligomer units are coparallel, thereby inducing

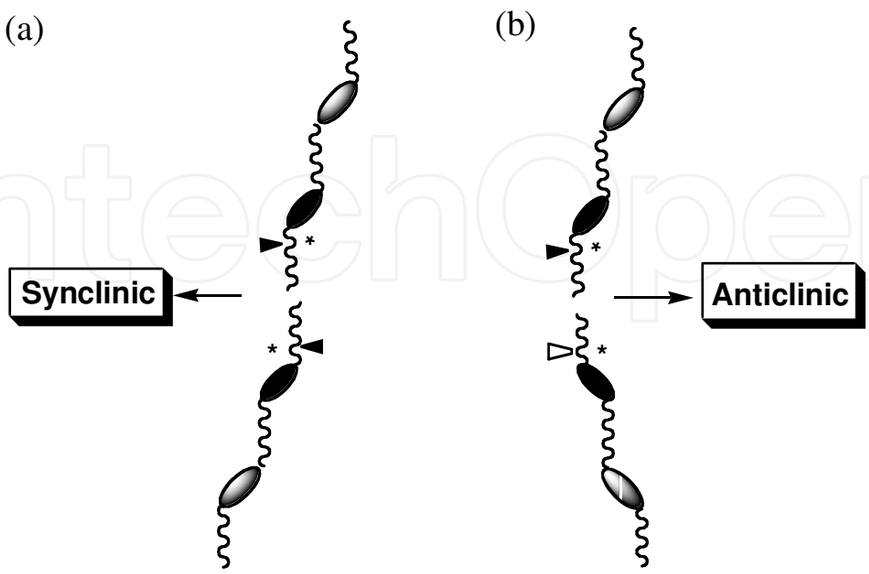

Fig. 20. Schematic sketches for (a) parallel twin ordering and (b) bent twin ordering via chiral interaction.

synclinic ordering. The other is a bent twin ordering in which they are inclined with respect to each other, inducing anticlinic ordering. The alkoxy tail substituted to the pyrimidine ring stabilizes the Ferri-L phase much more than the Ferri-H phase. Introduction of the alkoxy tail is thought to enhance the electrostatic dipole-quadrupole interaction and to stabilize the Ferri-L phase. The chiral dimeric system can induce favourable positional correlation among molecules in adjacent layers.

3.5.3 Molecular organization model

According to the theoretical study (Emelyanenko & Osipov 2003), ferrielectric phases are stabilized by two factors:

1. chirality-dependent direct polarization coupling between adjacent layers; and
2. electrostatic dipole-quadrupole interaction between positionally correlated molecules in adjacent layers.

Furthermore, our experimentally obtained results indicate that interlayer interaction via chiral recognition between preorganized molecules in adjacent layers is important for stabilization of the ferrielectric phases of the present dimesogenic system.

Figure 21 shows models for molecular organization in the Ferro, Ferri-H, Ferri-L, and Anti phases of the chiral system. A circle or cross is inserted at each interlayer region. Circles

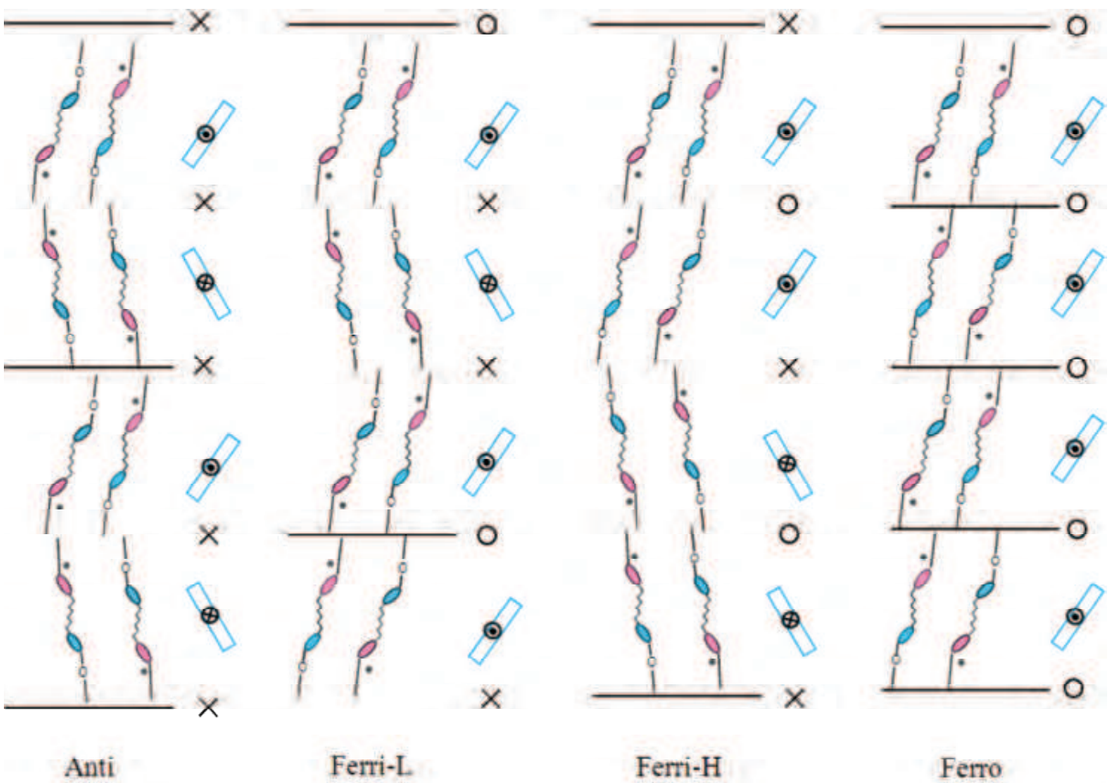

Fig. 21. Possible models for molecular organization in the Ferro, Ferri-H, Ferri-L, and Anti phases of the chiral system. The spontaneous polarization direction is indicated by arrows into or out of the page; the tilt direction is shown by solid lines. Open circles represent synclinic ordering in adjacent layers; crosses represent anticlinic ordering. The elliptical shapes represent mesogenic units within the molecules (Noji et al., 2009).

represent synclinic ordering in adjacent layers and crosses represent anticlinic ordering. In the Ferro phase, the tilt direction in each layer is the same between adjacent layers and polarization has the same direction. The Ferro phase consists of parallel twin orderings. In the Ferri-H phase, the two successive layers of the four periodic layers have the same tilt and polarization directions, whereas the other two layers have alternative ones. Such is the case for SmC*$_A$(1/2). The sequence of bent-parallel-bent-parallel-bent for the twin ordering is apparent at five nodes in the periodic four layers. The Ferri-H phase is destabilized by decreasing optical purity. Direct Iso-to-Ferri-H phase transition was observed for **(*R*)-II-(8,7)** possessing an alkoxy tail. These results suggest that chirality-dependent direct polarization coupling between adjacent layers is playing an important role in the stabilization of the Ferri-H phase. In the Ferr-L phase, two layers of the periodic three layers have the same tilt and polarization directions, although the other layer has alternative ones. Such is the case for SmC*$_A$(1/3). The sequence of parallel-bent-bent-parallel is apparent at four nodes in the periodic three layers. The stability of the Ferri-L phase was unaffected by macroscopic chirality. However, introduction of an alkoxy tail instead of an alkyl tail stabilizes the Ferri-L phase. Stabilization of the Ferri-L phase might therefore be governed by electrostatic dipole-quadrupole interaction in addition to microscopic chiral recognition. In the Anti phase, tilt and polarization directions are alternated between adjacent layers. The antiferroelectric phase consists of bent twin orderings.

With respect to the dimesogenic compounds with an odd-numbered spacer, many of bent conformers are converted to a linear form at the transition to the liquid-crystalline phase. This conversion accompanies a *trans* to *gauche* conformational change for some methylene units in the spacer. The orientational order organized by the interlayer interactions of the present frustrated phases is enhanced by the energetically unfavourable conversion.

4. Conclusion

We prepared a homologous series of chiral dimesogenic compounds and investigated their structure-property relations. The dimesogenic compounds possessing an even-numbered spacer show the Ferri-H and Ferri-L phases, whereas those possessing an odd-numbered spacer show the Ferri-L phase. The Ferri-H and Ferri-L phases were found to have a four-layer periodicity as SmC*$_A$(1/2) and a three-layer periodicity as SmC*$_A$(1/3), respectively. Large entropy changes at the Iso-to-Ferro phase transition were observed not only for the even-members but also for the odd-members, indicating that both members form a linear shape in which two mesogenic units are coparallel mutually in their ferrielecetric phases. Therefore, they have a preorganized structure in which an inherent tilt exists. The Ferri-H phase is destabilized by decreasing optical purity. However, the stability of the Ferri-L phase is unaffected by optical purity. Significant differences were found in chiral effect on the stabilization of a ferrielectric phase between Ferri-H and Ferri-L phases. Chirality-dependent direct polarization between adjacent layers is playing an important role in the stabilization of the Ferri-H phase. The stability of the Ferri-L phase is governed by interlayer interaction via microscopic chiral recognition between the preorganized molecules in adjacent layers. Furthermore, the induced positional correlation between molecules in adjacent layers can enhance interlayer dipole–quadrupole interaction to stabilize the Ferri-L phase. Our findings yield fundamental insights into the nature of long-range interaction producing clinicity in ferroelectric liquid

crystals in addition to a new approach to molecular design for supermolecules exhibiting a hierarchical phase structure.

5. Acknowledgments

We thank Professors J. Yamamoto and Y. Takanishi for X-ray measurements. We also thank Dr. I. Nishiyama for fruitful discussion. This work was partially supported by a Grant-in-Aid for Scientific Research (B) from the Japan Society for the Promotion of Science (No. 22350078) and a Grant for Hirosaki University Institutional Research.

6. References

Aoki, T.; Chao, Ke.; Fukuda, A.; Takanishi, Y.; Ishikawa, K.; Takezoe, H. & Nguyen, H. T. (1999). Antiferroelectricity of a Phase with the Four-Layered Periodicity that was Confirmed by Resonant X-ray Scattering, *Proceedings of 1999 Japanese Liquid Crystal Conference*, pp. 110-111, Toyama, Japan, September 29 – October 1, 1999.

Cepic, M. & Zeks, B. (2001). Flexoelectricity and Piezoelectricity: The Reason for the Rich Variety of Phases in Antiferroelectric Smectic Liquid Crystals. *Phys. Rev. Lett.* Vol. 87, 085501/1-4, ISSN 1079-7114.

Cepic, M.; Gorecka, E.; Pociecha, D.; Zeks, B. & Nguyen, H.T. (2002). Theoretical and Experimental Study of the Intermediate Sm C*FI2 and the Sm C*FI1 Phases in Antiferroelectric Liquid Crystals. *J. Chem. Phys.,* Vol. 117, pp. 1817-1826, ISSN 1089-7690.

Chandani, A. D. L.; Gorecka, E.; Ouchi, Y.; Takezoe, H. & Fukuda, A. (1989a). Antiferroelectric Chiral Smectic Phases Responsible for the Tristable Switching in MHPOBC. *Jpn. J. Appl. Phys*., Vol. 28, pp. L1265-L1268, ISSN 1347-4065.

Chandani, A. D. L.; Ouchi, Y.; Takezoe, H.; Fukuda, A.; Terashima, K.; Furukawa, K. & Kishi, K. (1989b). Novel Phases Exhibiting Tristable Switching. *Jpn. J. Appl. Phys.,* Vol. 28, pp. L1261-L1264, ISSN 1347-4065.

Emelyanenko, A.V. & Osipov, M.A. (2003). Theoretical Model for the Discrete Flexoelectric Effect and a Description for the Sequence of Intermediate Smectic Phases with Increasing Periodicity. *Phys. Rev. E,* Vol. 68, 051703/1-16, ISSN 1550-2376.

Fukuda, A.; Takanishi, Y.; Isozaki, K. & Takezoe, H. (1994). Antiferroelectric Chiral Smectic Liquid Crystals. *J. Mater. Chem.*, Vol. 4, pp. 997-1016, ISSN 1364-5501.

Fukui, M.; Orihara, H.; Yamada, Y. & Ishibashi, Y. (1989). New Phases in the Ferroelectric Liquid Crystal MHPOBC Studied by Differential Scanning Calorimetry. *Jpn. J. Appl. Phys.*, Vol. 28, pp. 849-850, ISSN 1347-4065.

Goodby, J.W.; Blinc, R.; Clark, N.A.; Largerwall, S.T.; Osipov, M.A.; Pikin, S.A.; Sakurai, T.; Yoshino, K. & Seks, B. (1991). Ferroelectric Liquid Crystals: Principles, Properties and Applications, pp. 166, 167, and 19-192, ISBN 2-88124-282-0, Philadelphia, Gordon & Breach.

Goodby, J.W.; Patel, J.S. & Chin, E. (1992). Ferroelectric, Ferrielectric and Antiferroelectric Properties in the (*R*)- and (*S*)-1-Methylalkyl 4′-(4′′-*n*-alkoxybenzoyloxy) biphenyl-4-carboxylate Liquid Crystals. *J. Mater. Chem.,* Vol. 2, pp. 197-207, ISSN 1364-5501.

Gorecka, E.; Chandani, A.D.L.; Ouchi, Y.; Takezoe, H. & Fukuda, A. (1990). Molecular Orientational Structures in Ferroelectric, Ferrielectric and Antiferroelectric Smectic Liquid Crystal Phases as Studied by Conoscope Observation. *Jpn. J. Appl. Phys.,* Vol. 29, pp. 131-137, ISSN 1347-4065.

Gorecka, E.; Pociecha, D.; Cepic, M.; Zeks, B. & Dabrowski, R. (2002). Enantiomeric Excess Dependence of the Phase Diagram of Antiferroelectric Liquid Crystals. *Phys. Rev. E* Vol. 65, 061703/1-4, ISSN 1550-2376.

Imrie, C. T. & Luckhurst, G. R. (1998). Liquid Crystal Dimers and Oligomers, *Handbook of Liquid Crystals* Vol. 1, Demus, D. ; Goodby, J. W. ; Gray, G. W. ; Spiess, H. -W. & Vill, V. (Eds), pp. 801-833, ISBN 3-527-29296-9, Weinheim, Wiley-VCH.

Inui, S.; Iimura, N.; Suzuki, T.; Iwane, H.; Miyachi, K.; Takanishi, Y. & Fukuda, A. (1996). Thresholdless Antiferroelectricity in Liquid Crystals and Its Application to Displays. *J. Mater. Chem.,* Vol. 6, pp. 671-673, ISSN 1364-5501.

Isozaki, T.; Fujisawa, T.; Takezoe, H.; Fukuda, A.; Hagiwara, T.; Suzuki, Y. & Kawamura, I. (1992) Competition between Ferroelectric and Antiferroelectric Interactions Stabilizing Varieties of Phases in Binary Mixtures of Smectic Liquid Crystals. *Jpn. J. Appl. Phys*., Vol. 31, pp. L1435-L1438, ISSN 1347-4065.

Isozaki, T.; Fujisawa, T.; Takezoe, H.; Fukuda, A.; Hagiwara, T.; Suzuki, Y. & Kawamura, I. (1993). Devil's Staircase Formed by Competing Interactions Stabilizing the Ferroelectric Smectic-C* Phase and the Antiferroelectric Smectic-C_A* Phase in Liquid Crystalline Binary Mixtures. *Phys. Rev. B,* Vol. 48, pp. 13439-13450, ISSN 1550-235X.

Jaradat, S.; Roberts, N. W.; Wang, Y.; Hirst, L.S. & Gleeson, H.F. (2006). Remarkably Wide Four-layer Smectic Phases in Mixtures of Liquid Crystals and Highly Chiral Dopants. *J. Mater. Chem.,* Vol. 16, pp. 3753-3761, ISSN 1364-5501.

Jaradat, S.; Brimicombe, P. D.; Roberts, N. W.; Southern, C.; Gleeson, H. F. (2008). Asymmetric Switching in a Ferrielectric Liquid Crystal Device. *Appl. Phys. Lett.,*Vol. 93, 153506/1-3, ISSN ISSN 1079-7114.

Jaradat, S.; Brimicombe, P. D.; Southern, C.; Siemianowski, S. D.; DiMasi, E.; Pindak, R. & Gleeson, H. F. (2009). Stable Field-induced Ferrielectric Liquid Crystal Phases in Devices. *Appl. Phys. Lett.,* Vol. 94, 153507/1-3, ISSN 1079-7114.

Johnson, P. M.; Olson, D. A.; Pankratz, S.; Nguyen, T.; Goodby, J. W.; Hird, M. & Huang, C. C. (2000). Structure of the Liquid-Crystal Ferrielectric Phases as Determined by Ellipsometry. *Phys. Rev. Lett.,* Vol. 84, pp. 4870-4873, ISSN 1092-0145.

Lemieux, R. (2007). Molecular Recognition in Chiral Smectic Liquid Crystals : The Effect of Core-Core Interactions and Chirality Transfer on Polar Order. *Chem. Soc. Rev*., Vol. 36, 2033-2045, ISSN 1460-4744.

Lagerwall, J. P. F. & Giesselmann, F. (2006). Current Topics in Smectic Liquid Crystals Research. *ChemPhysChem*., Vol. 7, pp. 20-45, ISSN 1439-7641.

Mach, P.; Pindak, R.; Levelut, A. –M.; Barois, P.; Nguyen, H. T.; Huang, C. C. & Furenlid, L. (1998). Structural Characrarization of Various Chiral Smectic- *C* Phases by Resonant X-Ray Scattering. *Phys. Rev. Lett.,* Vol. 81, pp. 1015-1018, ISSN 1092-0145.

Mach, P.; Pindak, R.; Levelut, A. –M.; Barois, P.; Nguyen, H. T.; Baltes, H.; Hird, M.; Seed, A. J.; Goodby, J. W.; Huang, C. C. & Furenlid, L. (1999). Structures of Chiral Smectic-*C*

Mesophases Revealed by Polarization-Analyzed Resonant X-Ray Scattering. *Phys. Rev. E*, Vol. 60, pp. 6793-6802, ISSN 1550-2376.

Matsumoto, T.; Fukuda, A.; Johno, M.; Motoyama, Y.; Yui, T.; Seomun, S.-S. & Yamashita, M. (1999). A Novel Property Caused by Frustration Between Ferroelectricity and Antiferroelectricity and Its Application to Liquid Crystal Displays— Frustoelectricity and V-Shaped Switching. *J. Mater. Chem.,* Vol. 9, pp. 2051-2080, ISSN 1364-5501.

Nguyen, H. T.; Rouillon, J. C.; Cluzeau, P.; Sigaud, G.; Destrade, C. & Isaert, N. (1994).New Chiral Thiobenzoate Series with Antiferroelectric Mesophases, *Liq. Cryst.,* Vol. 17, pp. 571-583, ISSN 1366-5855.

Nishiyama, I.; Yamamoto, J.; Goodby, J.W. & Yokoyama, H. (2001). A Symmetric Chiral Liquid-Crystalline Twin Exhibiting Stable Ferrielectric and Antiferroelectric Phases and a Chirality-Induced Isotropic–Isotropic Liquid Transition. *J. Mater. Chem.,* Vol. 11, pp. 2690-2693, ISSN 1364-5501.

Nishiyama, I. (2010). Remarkable Effect of Pre-organization on the Self Assembly in Chiral Liquid Crystals, *The Chemical Record*, Vol. 9, pp. 340-355, ISSN 1528-0691.

Noji, A.; Uehara, N.; Takanishi, Y.; Yamamoto, J. & Yoshizawa, A. (2009). Ferrielectric Smectic C Phases Stabilized Using a Chiral Liquid Crystal Oligomer. *J. Phys. Chem. B,* Vol. 113, pp. 16124-16130, ISSN 1520-5207.

Noji, A. & Yoshizawa, A. (2011). Isotropic Liquid-Ferrielectric Smectic C Phase Transition Observed in a Chiral Nonsymmetric Dimer. *Liq. Cryst.*, Vol. 38, pp. 451-459., ISSN 1366-5855.

Osipov, M. A. & Fukuda, A. (2000). Molecular Model for the Anticlinic Smectic-C_A Phase *Phys. Rev. E,* Vol. 62, pp. 3724-3735, ISSN 1550-2376.

Sandhya, K.L.; Vij, J.K.; Fukuda A. & Emelyanenko, A.V. (2009). Degeneracy Lifting Near the Frustration Points Due to Long- Lange Interlayer Interaction Forces and the Resulting Varieties of Polar Chiral Tilted Smectic Phases. *Liq. Cryst.,* Vol. 36, pp. 1101-1118, ISSN 1366-5855.

Takezoe, H.; Gorecka, E. & Cepic, M. (2010). Antiferroelectric Liquid Crystals: Interplay of Simplicity and Complexity. *Rev. Mod. Phys.,* Vol. 82, pp. 897-937, ISSN 1530-0756.

Walba, D. M. (1995). Fast Ferroelectric Liquid-Crystal Electrooptics. *Science*, Vol. 270, pp. 250-251, ISSN 1095-9203.

Wang, S.; Pan, L.; Pindak, R.; Liu, Z.Q.; Nguyen, H.T. & Huang, C.C. (2010). Discovery of a Novel Smectic-C* Liquid-Crystal Phase with Six-layer Periodicity. *Phys. Rev. Lett.,* Vol. 104, 027801/1-4, ISSN 1092-0145.

Yamashita, M. & Miyajima, S. (1993). Successive Phase Transition – Ferro-, Ferri-and Antiferro-Electric Smectics. *Ferroelectrics,* Vol. 148, pp. 1-9, ISSN 1563-5112.

Yoshizawa, A. Nishiyama, I. ; Fukumasa, M. ; Hirai, T. & Yamane, M. (1989). New Ferroelectric Liquid Crysal with Large Spontaneous Polarization. *Jpn. J. Appl. Phys.*, Vol. 28, pp. L1269-L1271, ISSN 1347-4065.

Yoshizawa, A ; Kikuzaki, H. & Fukumasa, M. (1995). Microscopic Organization of Molecules in Smectic A and Chiral (Racemic) Smectic C Phases : Dynamic Molecular Deformation Effect on the S_A to S_C* (S_C) Transition. *Liq. Cryst.*, Vol. 18, pp. 351-366, ISSN 1366-5855.

Yoshizawa A. & Nishiyama I. (1995). Interlayer Correlation in Smectic Phases Induced by Chiral Twin Molecules. *Mol. Cryst. Liq. Cryst.*, Vol. 260, pp. 403-422, ISSN 1563-5287.

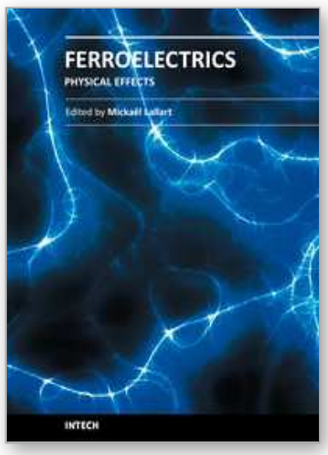

Ferroelectrics - Physical Effects

Edited by Dr. MickaÃ«l Lallart

ISBN 978-953-307-453-5
Hard cover, 654 pages
Publisher InTech
Published online 23, August, 2011
Published in print edition August, 2011

Ferroelectric materials have been and still are widely used in many applications, that have moved from sonar towards breakthrough technologies such as memories or optical devices. This book is a part of a four volume collection (covering material aspects, physical effects, characterization and modeling, and applications) and focuses on the underlying mechanisms of ferroelectric materials, including general ferroelectric effect, piezoelectricity, optical properties, and multiferroic and magnetoelectric devices. The aim of this book is to provide an up-to-date review of recent scientific findings and recent advances in the field of ferroelectric systems, allowing a deep understanding of the physical aspect of ferroelectricity.

InTech Europe
University Campus STeP Ri
Slavka Krautzeka 83/A
51000 Rijeka, Croatia
Phone: +385 (51) 770 447
Fax: +385 (51) 686 166
www.intechopen.com

InTech China
Unit 405, Office Block, Hotel Equatorial Shanghai
No.65, Yan An Road (West), Shanghai, 200040, China
中国上海市延安西路65号上海国际贵都大饭店办公楼405单元
Phone: +86-21-62489820
Fax: +86-21-62489821

IntechOpen